

# We are IntechOpen, the world's leading publisher of Open Access books Built by scientists, for scientists

6,900

Open access books available

186,000

International authors and editors

200M

Downloads

Our authors are among the

154

Countries delivered to

TOP 1%

most cited scientists

12.2%

Contributors from top 500 universities



WEB OF SCIENCE™

Selection of our books indexed in the Book Citation Index  
in Web of Science™ Core Collection (BKCI)

Interested in publishing with us?  
Contact [book.department@intechopen.com](mailto:book.department@intechopen.com)

Numbers displayed above are based on latest data collected.  
For more information visit [www.intechopen.com](http://www.intechopen.com)



# Overview on Stereoscopic Particle Image Velocimetry

L. Martínez-Suástegui

*ESIME Azcapotzalco, Instituto Politécnico Nacional, Colonia Santa Catarina,  
Delegación Azcapotzalco, México, Distrito Federal,  
Mexico*

## 1. Introduction

Recently, Particle Image Velocimetry (PIV) has become the method of choice for multiple fluid-dynamic investigations (Adrian 1991; Willert and Gharib 1991; Jakobsen, Dewhurst et al. 1997; Westerweel 1997; Raffel, Willert et al. 1998). PIV is a reliable non-intrusive laser optical measurement technique that is based on seeding a flow field with micron-sized tracer particles and illuminating a two-dimensional (2D) slice or target area with a laser light sheet (Adrian and Yao 1985; Melling 1997). The target area is captured onto the sensor array of a digital camera, which is able to capture each light pulse in separate image frames. After recording a sequence of two light pulses, velocity vectors are derived from small subsections (called interrogation areas) of the target area of the particle-seeded flow by measuring the distance travelled by particles in the flow within a known time interval. The interrogation areas from the two image frames are cross-correlated with each other, pixel by pixel, producing a signal peak that allows for an accurate measurement of the displacement, and thus the velocity. Finally, the instantaneous velocity vector map over the whole target area is obtained by repeating the cross-correlation for each interrogation area over the two image frames captured by the camera (Nishino, Kasagi et al. 1989; Keane and Adrian 1992; Mao, Halliwell et al. 1993; Westerweel, Dabiri et al. 1997). The major drawback of the 2D PIV technique is that it records only the projection of the velocity vector into the plane illuminated by the laser sheet, so the out-of-plane velocity component is lost and the in-plane components are affected by an unrecoverable error due to the perspective transformation. Although the “classical” PIV method introduces an error due to the perspective projection and uncertainty in measuring the in-plane velocity components, most of the time it is commonly neglected, since it still allows the user to interpret the instantaneous flow field and its structures (Lawson and Wu 1997; Lawson and Wu 1997; Soloff, Adrian et al. 1997). Unfortunately, this is not the case when studying highly three-dimensional flows, where the only way to avoid the uncertainty error is to measure all three components of the velocity vectors using stereoscopic techniques (Adrian 1991; Arroyo and Greated 1991; Westerweel and Nieuwstadt 1991; Hinsch 1993; Prasad and Adrian 1993; Raffel, Gharib et al. 1995; Lawson and Wu 1999; Prasad 2000; Doorne 2004; Tatum, Finnis et al. 2005; Mullin and Dahm 2006; Tatum, Finnis et al. 2007). Stereoscopic PIV uses two cameras with separate viewing angles. By combining the two velocity fields measured by

each camera using geometrical equations derived from the camera setup and a complicated calibration step, the third velocity component is evaluated and a three-dimensional (3D) velocity field is achieved (Nishino, Kasagi et al. 1989; Grant, Zhao et al. 1991; Raffel, Gharib et al. 1995; Willert 1997; Kähler and Kompenhans 2000; Shroder and Kompenhans 2004; Mullin and Dahm 2005; Perret, Braud et al. 2006).

In the present chapter, the technical basis, the set-up and components of a stereoscopic PIV apparatus/equipment are described so that the reader can understand how the different items of equipment are combined to form a coherent PIV tool (Hu, Saga et al. 2001). Afterwards, the principles of stereo PIV calibration, data acquisition, processing, and analysis are addressed. The aim of this chapter is to present in a more general context the aspects of the PIV technique relevant for those who intend to purchase a stereoscopic PIV system or those who want to perform stereoscopic PIV measurements. By understanding how to plan and perform experiments, it is hoped that it will allow the reader to successfully design a custom measurement system to fit a specific scientific or industrial application. In addition, this chapter will prove a valuable tool for those who already own a 2D PIV system and want to upgrade it for 3D measurement acquisition.

## 2. PIV system overview

There are several commercial stereoscopic PIV systems available, but the basic elements of these systems must include the following items: a pulsed laser system, two cameras for stereoscopic measurements, and a PC connected to a data acquisition card that synchronizes all of these items. The instrumentation required to perform the PIV data acquisition process is seeding, illuminating, recording, processing, and analysing the flow field. One drawback of PIV systems is that all of these items contribute to each stage of the measurement process, and therefore none of them can be spared. A brief description of the aforementioned instrumentation is presented in the following subsections.

### 2.1 Illumination systems

A stroboscopic light-sheet is desired to illuminate the plane of interest. This can be generated with pulsed lasers, continuous wave lasers, electro-optical shutters, polygon scanners, light guides and optical assemblies. Since only pulsed lasers have sufficient energy to record particle images, for relatively high speed flows seeded with micron or submicron particles, the most common choice are Nd:Yag lasers with a wavelength of 532 nm, since they offer repetition rates that match most of the commercially available CCD cameras. Pulsed laser systems include an array of optics with several cylindrical lenses that produces a diverging light sheet with adjustable thickness. This optical system includes an optical mount that can rotate through 360°. One thing to remember when designing experiments is that in order to avoid damage to the equipment, the laser must always be mounted and operated in a horizontal position. The sheet can be easily oriented by deflecting the laser beam using a mirror. Also, when it comes to choosing a pulsed laser for a stereo PIV system, the most important specifications to account for are: minimum sheet thickness range, the sheet focusing range, the maximum input pulse energy, the maximum input beam diameter, and of course its dimensions. The laser of choice must suit the measurement of the particular flow field under investigation. Nevertheless, when purchasing a PIV system, always aim for a laser with the maximum laser power output.

## 2.2 Cameras

Several CCD-based cameras are currently available. They differ in the desired spatial resolution, temporal resolution, directional ambiguity resolution, and cross-correlation options. Again, the cameras of choice depend on the resolution of the spatial and temporal features of the flow field to be measured. Generally, as the spatial resolution of the camera increases, its temporal resolution decreases. Therefore, when customizing your PIV equipment, always make sure that the chosen cameras meet the following criteria. They have enough temporal resolution in order to resolve the smallest velocity displacements between the first and second images of the particles of the flow field under investigation. The size of the smallest velocity structures can be measured in the flow field under study. One important thing to consider is that commercial PIV systems include a feature that interfaces the input buffer in the PIV processor with the cameras, thus allowing future upgrades of particular camera systems that better suit your needs. With that in mind, the best option when purchasing your first set of cameras for the PIV system is to make sure that they satisfy your particular needs in terms of temporal resolution with the highest spatial resolution.

## 2.3 Software to perform the PIV data acquisition process

The software of the PIV system must include a synchronization unit that links signals to and from the processor, the laser and cameras. Once the images have been acquired, the system must be able to produce and store vector maps or image maps in a database on a hard disc of a PC that keeps track of both the data and corresponding data acquisition and analysis parameters used.

## 2.4 3D traverse system

If the light sheet optics and the cameras are mounted on a common traverse system, they can be positioned at any desired point in the flow domain. This capability is particularly advantageous for measuring image data at multiple planes in a flow. Volume mapping is a technique based on performing multiple 3D stereoscopic PIV mappings in cross-sections of a flow within a very short time interval (Meinhart, Wereley et al. 2000; Klank, Goranovic et al. 2001). Unfortunately, this technique can only be used with a traverse system, and it is achieved by mounting the laser cavity and the cameras on an electronically controlled traverse system. In this way, when the entire traverse system is moved, the distance between the cameras and the light sheet remains constant so that there is no need to calibrate again. Although 2D or 3D PIV measurements can be performed without a traverse system, the main advantage of these systems is that they allow for fast and accurate calibration. For stereoscopic measurements in an enclosed flow (e.g., a duct flow, where the laser and cameras are outside of a transparent model), the index of refraction can have a strong effect on the calibration. One method to ensure that the two cameras have an orthogonal orientation with respect to the liquid-air interface is to redesign the wall of the test section to incorporate a triangular prismatic section. This is easily achieved by constructing a glass container that is filled with the same liquid and that is attached to the test section. By using a liquid prism between the test section and the lens of each camera, orthogonal viewing is accomplished with respect to the liquid-air interface and the aberrations are minimized (Prasad and Adrian 1993; Prasad and Jensen 1995). Also, when the test section has curved walls, distortion caused by refraction is minimized by enclosing the test section in a container with flat windows and filled with the same fluid as the test section.

### 3. Stereoscopic PIV calibration tools

In this section, the calibration tools for stereoscopic calibration and the calibration procedure are presented and described in detail.

#### 3.1 Camera mounts for stereoscopic viewing

In most 3D PIV systems, when viewing the light sheet at an angle, the camera's entire field of view must be accurately focused. This is known as the Scheimpflug condition, and it is accomplished using camera mounts that include angle adjustment so that the image plane (CCD-plane), lens plane and object plane for each of the cameras intersect at a common point, as shown in Figure 1a (Scheimpflug 1904; Prasad and Jensen 1995; Zang and Prasad 1997). Figure 1b shows a camera mounted on a stereoscopic camera mount with angle adjustment and Scheimpflug condition.

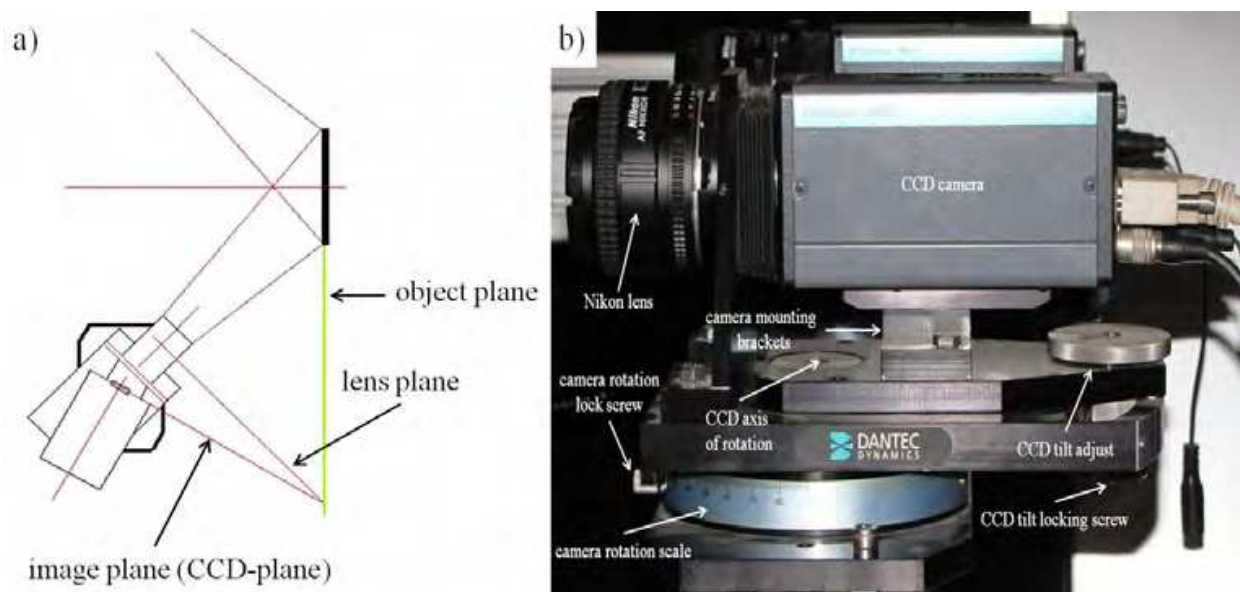


Fig. 1. a) Scheimpflug camera. b) CCD camera mounted on a Scheimpflug camera mount.

#### 3.2 Calibration target

Stereo PIV measures displacements by using two cameras playing the role of eyes. By comparing the images of each camera against a calibration target, a stereoscopic calibration, which will be described in the next subsection, is achieved. Plane calibration targets consist of a one-sided white image with black dots on a regular spaced grid that is easily detected using image processing techniques (Harrison, Lawson et al. 2001; Ehrenfried 2002; Wieneke 2005). When these targets are used, the two cameras have to be positioned on the same side. On the other hand, double-sided (multi-level) targets contain a two-level grid of white dots on a black background located at two different and known orientations of the  $z$ -axis, where  $z$  is the distance away from the camera(s). One major advantage of these targets is that depending on the configuration of the experimental setup, the user can choose to mount the cameras either on opposite sides of the calibration target or on the same side. Although small angles between the two cameras can be used, the out-of-plane displacement is obtained more accurately when a larger angle is used between the two cameras. In this sense, the most accurate calibration is obtained when the angle between the two cameras is

set to  $90^\circ$  (Sinha 1988; Westerweel and Nieuwstadt 1997). Nonetheless, stereoscopic PIV is also possible using a nonsymmetric arrangement of the cameras as long as the viewing axes are not collinear. Both types of targets have a larger centre dot called the “zero marker” which corresponds to the level at which the big dot in the centre of the calibration target is placed. Figure 2 shows the recommended setup for the cameras depending on the type of target used. Note that when the cameras have a narrow depth of field, a smaller separation angle will be needed to allow a wider field of view (i.e., where both cameras are in focus).

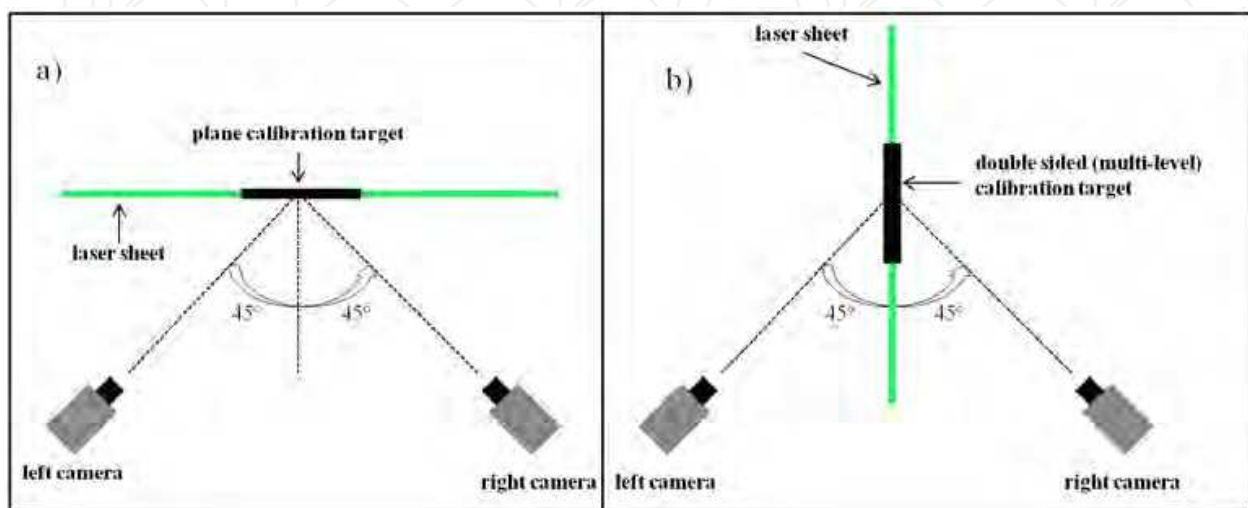


Fig. 2. Optimal camera configurations for an optimal determination of the stereoscopic calibration coefficients: a) Configuration using a plane (one-sided) calibration target. b) Configuration using a multi-level (two-sided) calibration target.

### 3.3 Calibration procedure

An imaging model describes the mapping of points from the image plane to object space, and the model parameters are determined through analysis of one or more calibration images. To obtain an imaging model, the first step is to accurately align the calibration target with the laser light sheet (Willert 1997). For 3D PIV measurements, the laser light thickness is adjusted by an optical arrangement supplied with the laser so that the illuminated plane is as thick as possible. If calibration is to be performed using a plane target, the cameras have to acquire images of the target through a number of  $z$  positions. This is generally accomplished by mounting the target on a special traverse unit and recording three to five  $z$  positions. Figure 3 shows the calibration grid images obtained by each camera for one  $z$  position using a plane calibration target of  $100 \times 100$  mm with black dots and white background. The camera configuration corresponds to the one shown in Figure 2a).

Multi-level double sided targets eliminate the need for traversing, since they contain a two-level grid of white dots on a black background with known dot spacing in the  $x, y$  and  $z$  positions. Figure 4 shows a multi-level target of  $270 \times 190$  mm with white dots and black background. The alignment of the laser light sheet and the target depend on the camera configuration. If the cameras are located on opposite sides of a multi-level calibration target, then the laser light sheet has to be aligned with the centre of the target. Here, the  $z=0$  coordinate is located at the centre of the laser light sheet. If the cameras are placed on the same side of the calibration target, the laser light sheet has to be positioned in the plane located in the middle of each level. In this case, the plane located at the centre of the light

sheet corresponds to the plane at which  $z=0$ . After aligning the calibration target, the user has to select the type of target used from a list. This setting allows the system to associate known  $x$  and  $y$  positions with the size and location of the markers, as the calibration algorithm automatically identifies the  $x$  and  $y$  coordinates on the images. The calibration target used during 3D stereo PIV measurements must always match the experimental setup, i.e. when measuring a large or small area, a large or small target is needed, respectively.

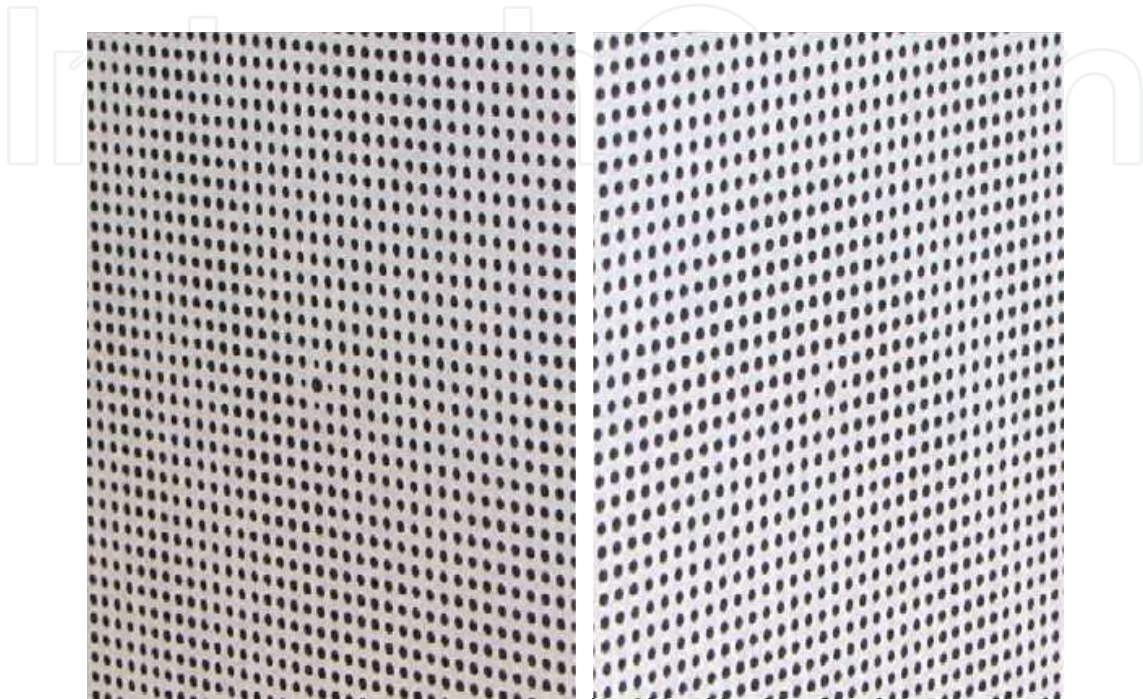


Fig. 3. Right and left calibration grid images obtained by each camera using a plane (one-sided) calibration target. The big dot in the centre of the calibration target is the zero marker.

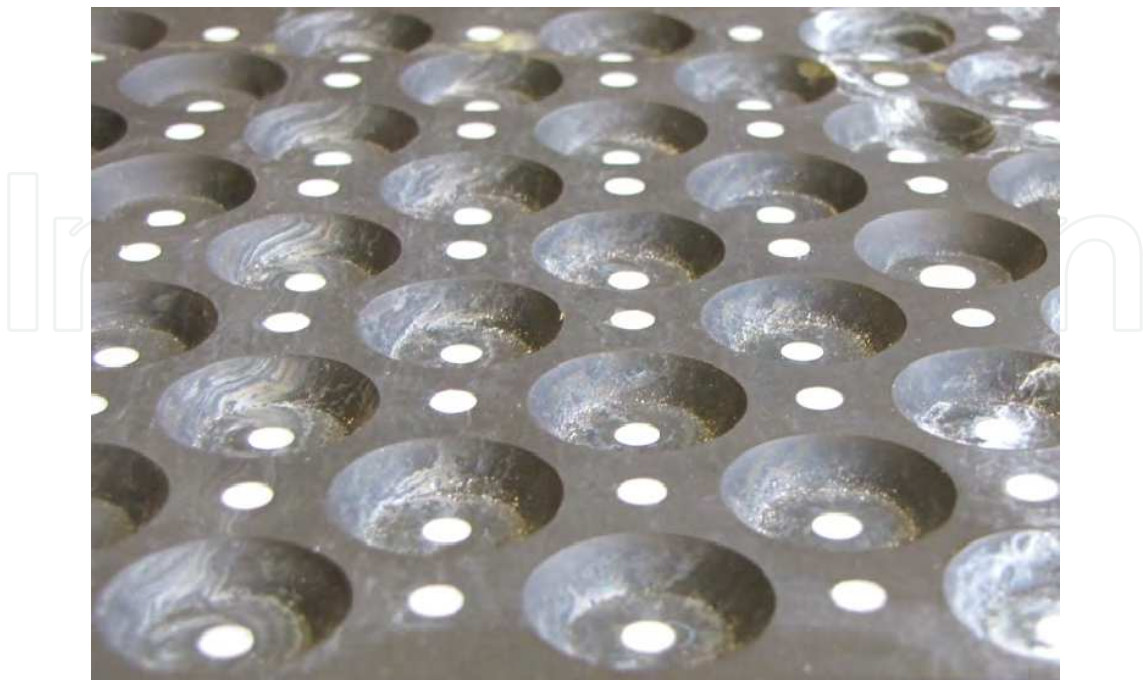


Fig. 4. Multi-level target of 270 x 190 mm with white dots and black background.

Once the type of target used for the calibration is entered, information such as dot spacing in the  $x$ ,  $y$  coordinates, zero marker diameter, axis marker diameter and level distance are known. The next step is to define the coordinate axes as seen from the cameras' point of view and the target configuration. Here, the  $x$ ,  $y$  and  $z$  axes are always horizontal, vertical, and normal to the light sheet, respectively. However, each can be positive in any direction so that eight different coordinate system combinations are available. To obtain the  $z$  calibration coefficient, each camera records images of the calibration target for several  $z$  positions by traversing it in a direction normal to the laser sheet. Each displacement value is entered by the user in the dataset properties, and this calibration stage determines the  $x$ - $y$  image to object plane space mapping (Lawson and Wu 1997; Soloff, Adrian et al. 1997). Table 1 shows some of the available sizes for each type of target. Note that for the case of multi-level targets, the  $z$ -coordinate refers to the location of the zero marker and the  $z$  values entered correspond to the dots located on the second level. These values are added or subtracted depending on the level spacing of each target and on how the calibration target is aligned with the laser light sheet.

Type of calibration target	Size (mm)	Z values entered (mm)
Dots	100 x 100	-
Dots	200 x 200	-
Dots	270 x 200	-
Dots	450 x 450	-
Multi-level	270 x 190	2 <sup>nd</sup> level +4
Multi-level	270 x 190	2 <sup>nd</sup> level -4
Multi-level	95 x 75	2 <sup>nd</sup> level +2
Multi-level	95 x 75	2 <sup>nd</sup> level -2

Table 1. Available sizes for plane and multi-level calibration targets.

After the entry properties of the calibration images are set and saved, the obtained transformation describes the overall perspective and lens distortion by providing parameter values for a specific image acquisition setup called the "imaging model fit". The calibration result can be verified by superimposing the model fit map to the corresponding calibration image. Figure 5 shows the imaging model for each camera based on an image size of 1344 x 1024 pixels after applying a direct linear transform and using a multi-level calibration target of 270 x 190 mm. The origin of the  $x$ ,  $y$  and  $z$  coordinates is located at the centre of the zero marker and the coordinate axes are displayed as seen from each camera. The yellow dots at the centre of the white markers appear when a successful image model fit is obtained. Note that for both images, the Scheimpflug condition was not accomplished on the markers located at each corner. Nonetheless, a successful 3D calibration can still be obtained using an image model fit using sixteen out of the twenty available markers.

The quality of the calculated imaging model fit can be evaluated with the value of the average reprojection error. The latter describes the average pixel distance from every marker found to the predicted image location (distance from the yellow dots at the centre of the white markers to the points of intersection of the green grid in Figure 5). In this sense, the

accuracy of the image model fit increases as the value of the average reprojection error decreases, and normally accepted values lie below 0.5. After performing a successful 3D calibration, the calibration target is removed and stereo measurements can be acquired by processing 2D PIV simultaneous recordings from each camera using the scale factor based on the image model fit. The two 2D vector maps recorded by each camera are then post processed using standard PIV processing software to obtain 3D vector maps. The main advantage of 3D calibration is that since a direct mapping function is derived between an object in 3D space and its corresponding location in the in-planes, there is no need to provide information regarding the geometric parameters of the stereoscopic image acquisition (Prasad 2000).

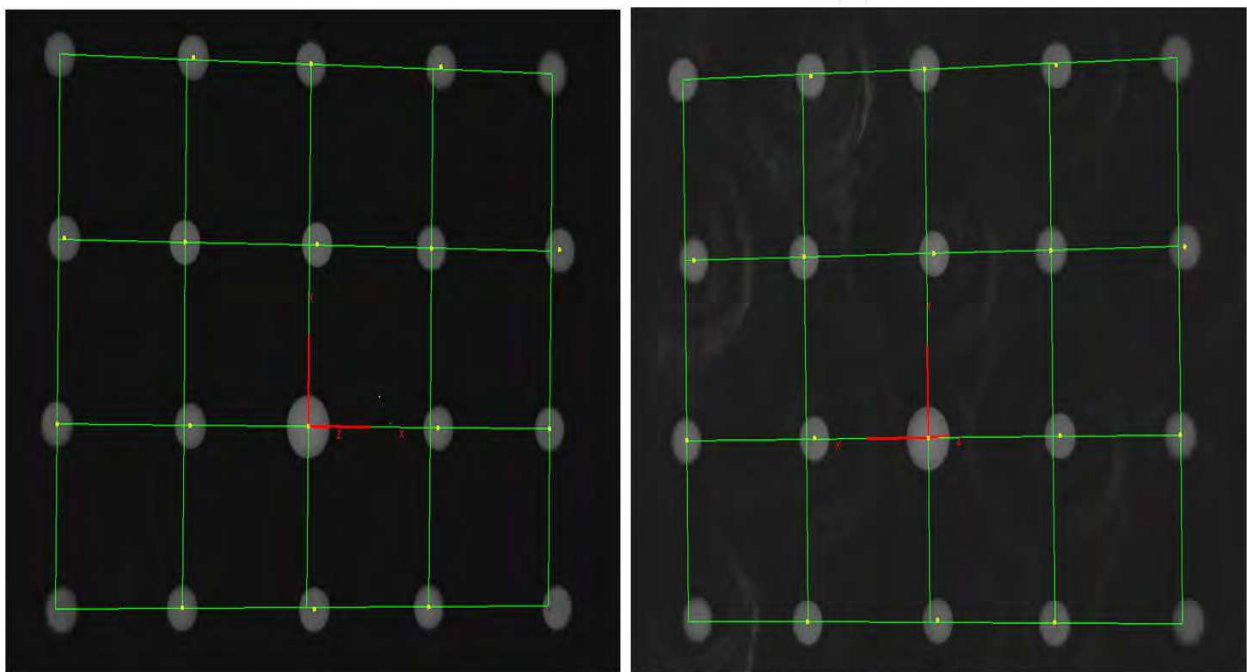


Fig. 5. Imaging model for each camera. The average reprojection errors are of  $1.5544 \times 10^{-1}$  and  $2.2423 \times 10^{-1}$  pixels for the left and right camera, respectively.

#### 4. Data processing and analysis

This section describes how to perform 3D data processing and analysis after data acquisition, and addresses various options to export the processed information of the 3D image maps for further investigation and processing to spreadsheet displays, ASCII files, MATLAB or Tecplot 360.

##### 4.1 Adaptive correlation

The adaptive correlation analysis method calculates velocity vectors starting with an initial interrogation area of size  $m \times n$  pixels. After the first iteration, vectors are recalculated using a smaller interrogation area, and this procedure is repeated until a final interrogation area is reached. The number of iterations is specified by the user and it's called "number of refinement steps." The size of the final interrogation area is also specified by the user, and its value is determined by entering values of the horizontal and

vertical sides (in pixels) of the latter. For each direction, available sizes are of 8, 16, 32, 64, 128 and 254 pixels. The initial interrogation area size is obtained by multiplying the final interrogation area size times the number of refinement steps, e.g., when selecting 3 refinement steps using a final interrogation area of 16 x 16 pixels, the initial interrogation area size is of 128 x 128 pixels. To reduce the correlation anomalies, overlap between neighbour interrogation areas can be specified independently for the horizontal and vertical directions. Validation parameters for the adaptive correlation method are normally used to remove spurious vectors. One of these parameters is the “peak validation.” Here, the user sets values for the minimum and maximum peak widths as well as the minimum peak height ratio between the first and second peak. The “local neighbourhood validation” rejects spurious vectors and replaces them using a linear interpolation method based on the surrounding vectors located at an area of  $m \times n$  pixels set by the user. Note that spurious vectors are identified by the inputted value of the “acceptance factor” parameter, and for larger values of this parameter, less velocity vectors are spatially corrected. The “moving average validation” method is used to validate vector maps by comparing each vector with the average of other vectors in a defined neighbourhood. Vectors that deviate from specified criteria are replaced using the average of the surrounding vectors. Figure 6 illustrates how the calculated velocity vectors obtained after applying an adaptive correlation can vary depending on the values of the input parameters described above. The computed vectors are displayed in blue, while the green vectors correspond to those obtained after interpolation with the surrounding vectors. This figure exemplifies the importance of adequately setting the values of the interrogation areas and validation methods employed. The instantaneous velocity map shown in Figure 6 is the recorded instantaneous flow structure of a free falling rotary seed that’s spinning at a stationary height inside a low-speed, vertical wind tunnel crafted for studying its flow and kinematics. Velocity measurements were performed using a Dantec Dynamics DSPIV system and the images were processed using Dantec Dynamics software (DynamicStudio version 3.0.69). Seeding was supplied from a smoke generator (Antari Z-1500II Fog Machine, Taiwan, ROC) placed at the tunnel intake, and seeding quantity was regulated by monitoring the output from the DSPIV system (particle size 1  $\mu\text{m}$ ). To elucidate the effects of the value of the input parameters, the recipe for the left and right adaptive correlations of Figure 6 are displayed on the left and right sides of Figure 7, respectively.

The adaptive correlation on the left of Figure 6 used the following parameters for the interrogation areas: final interrogation area size of 32 x 16 pixels in the horizontal and vertical directions, respectively, no overlap between neighbour interrogation areas, one refinement step, and an initial interrogation area size is of 64 x 32 pixels. The validation parameters used are: moving average validation with an acceptance factor of 0.15 with three iterations using a neighbourhood size of 3 x 3. The adaptive correlation on the right of Figure 6 used the following parameters for the interrogation areas: final interrogation area size of 32 x 32 pixels, 25% and 50% of horizontal and vertical overlap, respectively, and five refinement steps using an initial interrogation area size of 1024 x 1024 pixels. The validation parameters used are: minimum peak height relative to peak 2 of 1.2, moving average validation using 3 iterations using a neighbourhood size of 3 x 3 and an acceptance factor of 0.15.

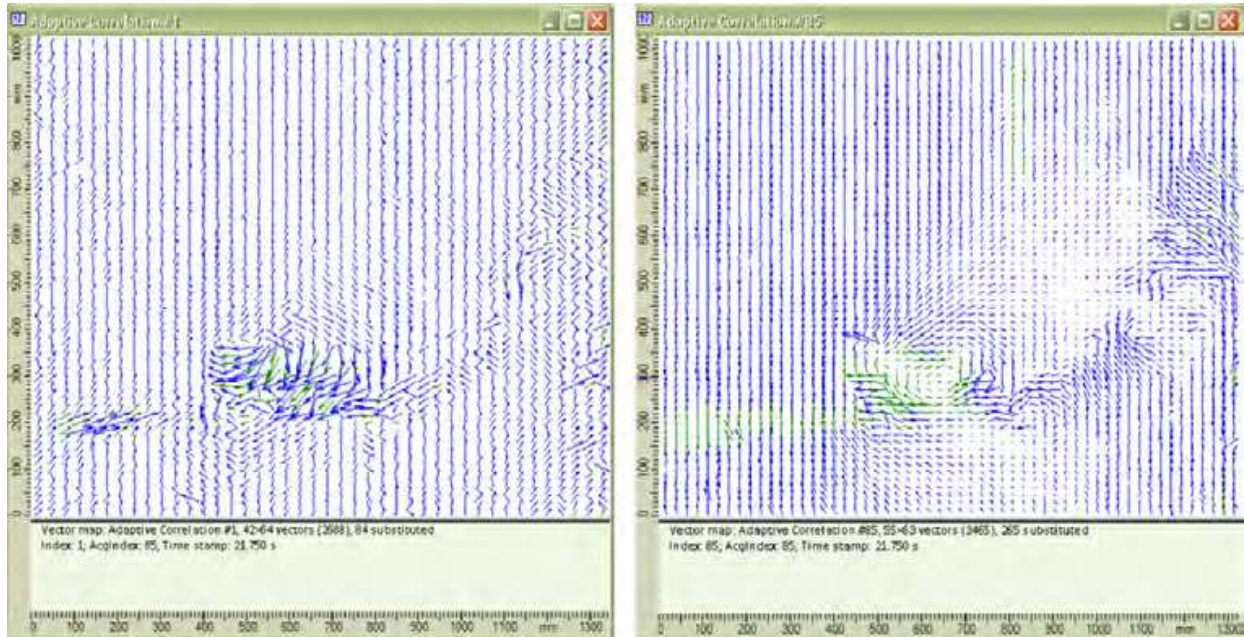


Fig. 6. Adaptive correlation applied to the same image pair by using different sizes of the final interrogation areas, number of refinement steps, and validation parameters.  
 Left image: 42 x 64 vectors, 2688 total vectors and 84 substituted vectors (green vectors).  
 Right image: 55 x 63 vectors, 3465 total vectors and 265 substituted vectors (green vectors).



Fig. 7. Adaptive correlation recipe used for the left image in Figure 6 (top and bottom left images), and adaptive correlation recipe used for the right image in Figure 6 (top and bottom right images).

#### 4.2 Average filter

This technique is used to filter and smooth vector maps. To apply this method, the user defines the size of the  $m \times n$  averaging area and an average vector is obtained based on the size of the averaging area size. Figure 8 shows how, after applying an average filter to the calculated velocity vectors, the instantaneous flow structure is smoothed. Note that a coherent structure is clearly visible at the centre of the right image. The recirculation shown corresponds to a leading-edge vortex (LEV) located on top of an autorotating airfoil.

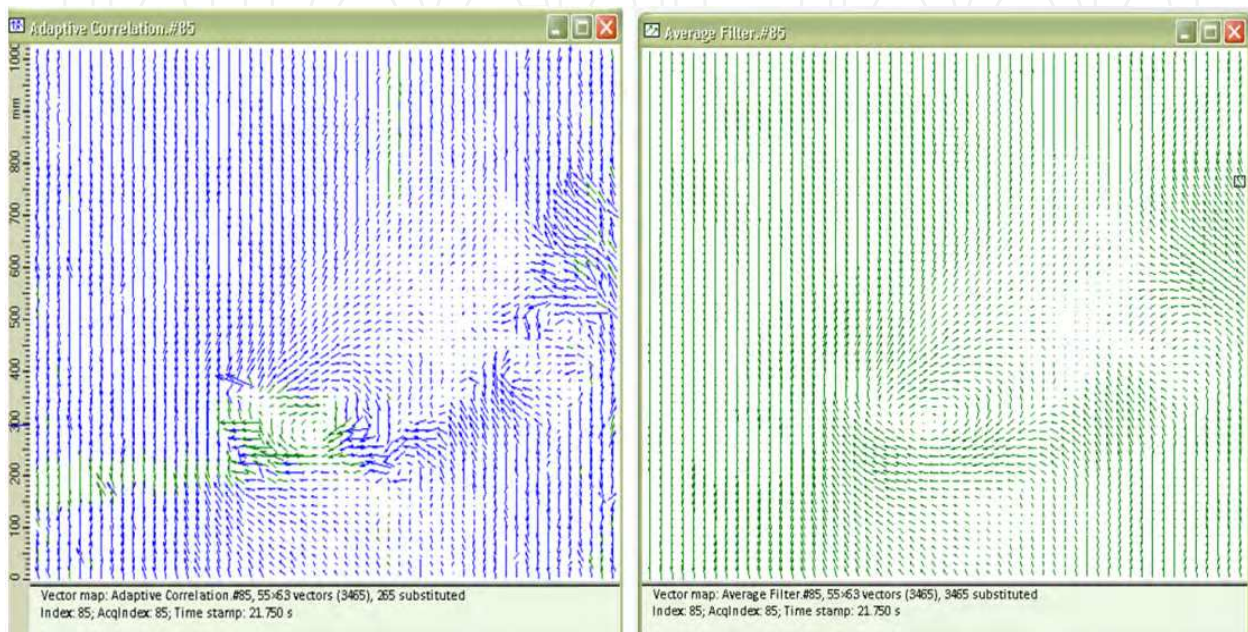


Fig. 8. Filtered instantaneous velocity map (right) after applying an average filter to the calculated velocity vectors (left) obtained using and adaptive correlation. The averaging area used is of  $7 \times 7$  pixels.

#### 4.3 Stereo PIV processing

As previously mentioned, the stereo PIV vector processing method computes 3D vectors based on the Imaging Model Fit obtained after stereoscopic calibration. To compute 3D vector maps, these steps must be followed: select the Image Model Fit and the 2D vector maps for each camera. Finally, apply the “Stereo Vector Processing” method from the PIV analysis group. Figure 9 illustrates how the resultant 3D PIV vector maps are layed out after applying the stereo vector processing method. Clearly, the flow field is displayed using traditional vector plots in 2D, and the scalar quantity of the out-of-plane velocity component is displayed with a scalar map and contours. Note that although the instantaneous 3D velocity field is obtained with this method, one major disadvantage is that the flow structure is still represented in the plane. Fortunately, commercial software from PIV systems has multiple options to export data to more powerful software packages for 3D flow visualization, such as MATLAB or Tecplot 360. Specifically, DynamicStudio from Dantec Dynamics includes a MATLAB link that transfers data of the recorded database to MATLAB’s workspace. In addition, results obtained can be transferred back to the DynamicStudio database after processing data in MATLAB.

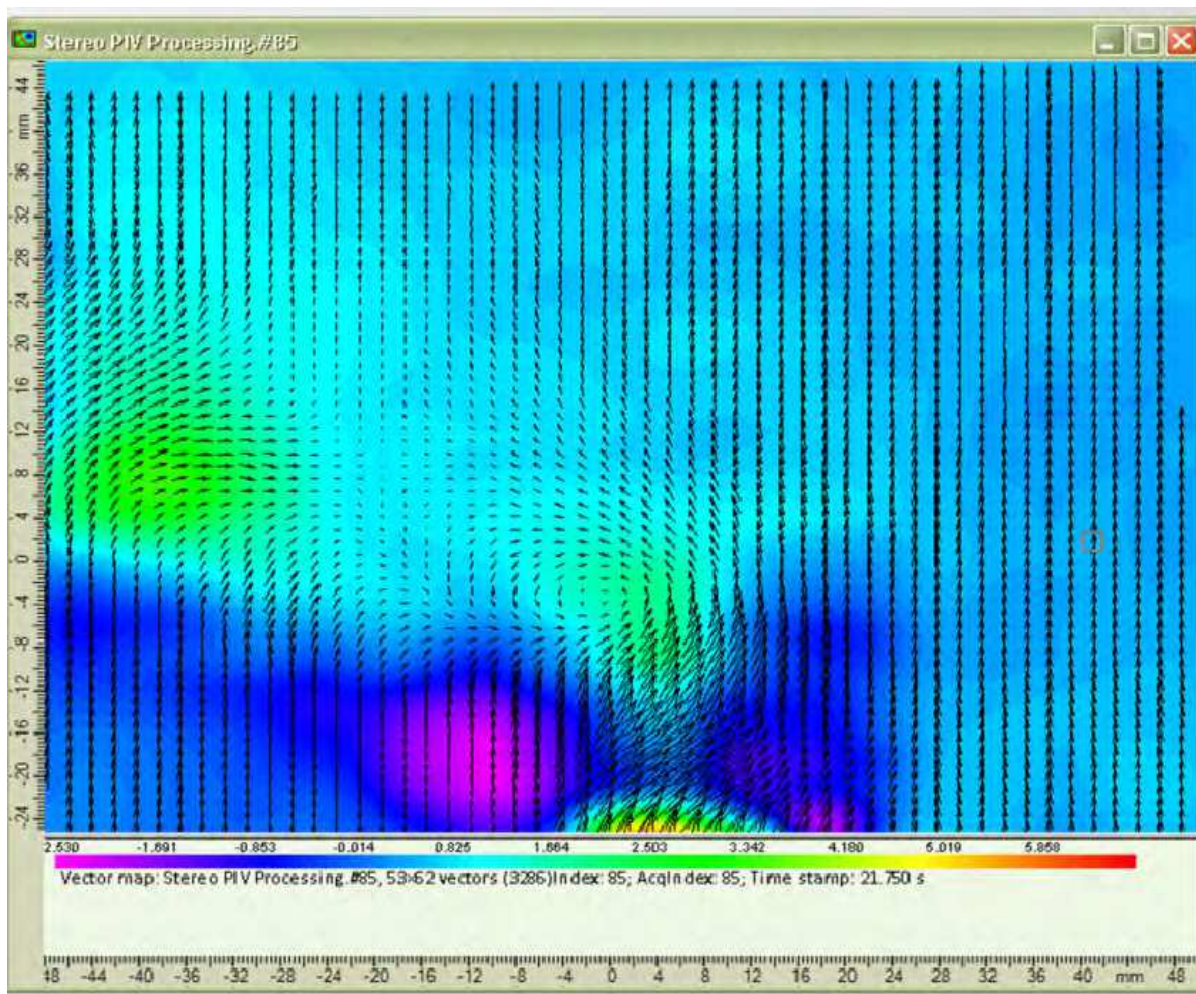


Fig. 9. 3D PIV vector map obtained after stereo PIV processing. The scale below the vector map illustrates the magnitude and direction of the out-of-plane velocity component.

#### 4.4 Scalar maps

Scalar maps are used to display on screen multiple data derived from the velocity fields. Examples of scalar maps that can be calculated are: contours for the  $u$ ,  $v$  and  $w$  velocity components, contours with gradients of the  $u$ ,  $v$  and  $w$  velocity components in the  $x$ ,  $y$  and  $z$  directions, vorticity contours, vortex identification methods, and the divergence of a 3D vector field. Figure 10 shows the vorticity contours for the instantaneous flow structure shown in Fig 9. In the next subsection, the steps to export databases for further processing using Tecplot 360 are presented.

#### 4.5 Exporting 3D vector maps for further processing using Tecplot 360

In this subsection, the steps to export data and reconstruct a three-component velocity field using Tecplot 360 are described. The first step is to select the 3D PIV vector fields and scalar maps to be exported. Afterwards, data are exported using a numerical export function. For Tecplot 360, the user specifies the path to the directory where data will be saved, chooses the names for the exported files, and saves them with a .DAT file extension. Finally, the

exported data files are loaded into Tecplot 360. Figure 11 displays the 3D instantaneous flow structure of Figure 9 and the vorticity contours of Figure 10 using Tecplot 360 after further processing. Figures 11a) and 11b) correspond to the frontal and rear perspectives normal to the plane of the laser sheet, respectively. The red circles enhance the location of the LEV and the trailing-edge vortex (TEV) close to the free falling rotary seed. Note how the LEV is visible using the front perspective, while the TEV is not. The opposite occurs for the rear perspective, where the TEV is visible but the LEV is not. Figure 12 shows the resulting flow structure after projecting the instantaneous 3D vector field of Figure 11 onto the plane illuminated by the laser sheet. Here, the vorticity contours are the same, but the size and location of the LEV, the TEV, and the overall flow structure changes dramatically. This exemplifies why 2D PIV measurements are prone to error when studying pronounced 3D flows, and hence, the importance of knowing the stereoscopic particle image velocimetry technique.

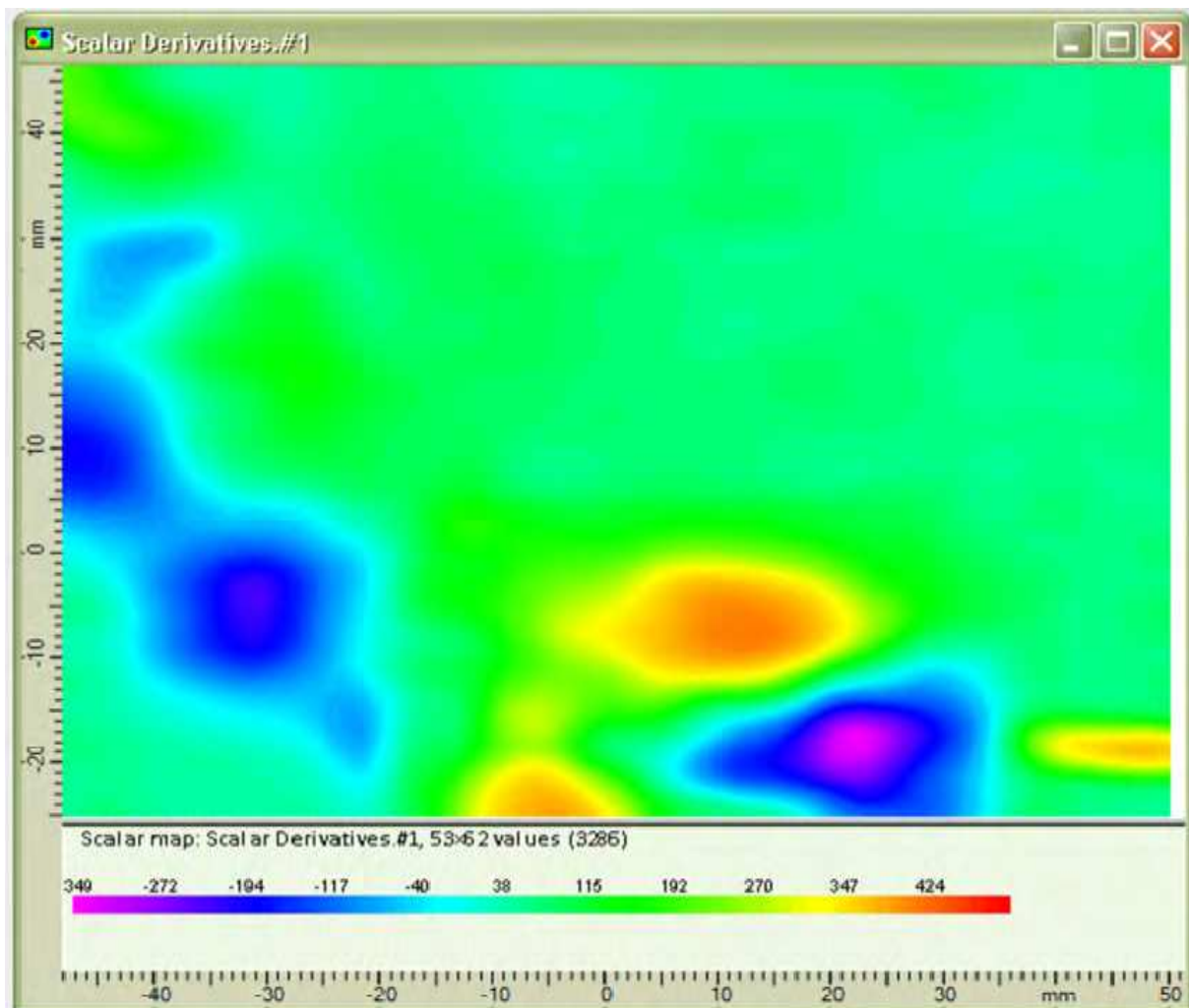


Fig. 10. Vorticity contours for the instantaneous flow structure shown in Figure 9.

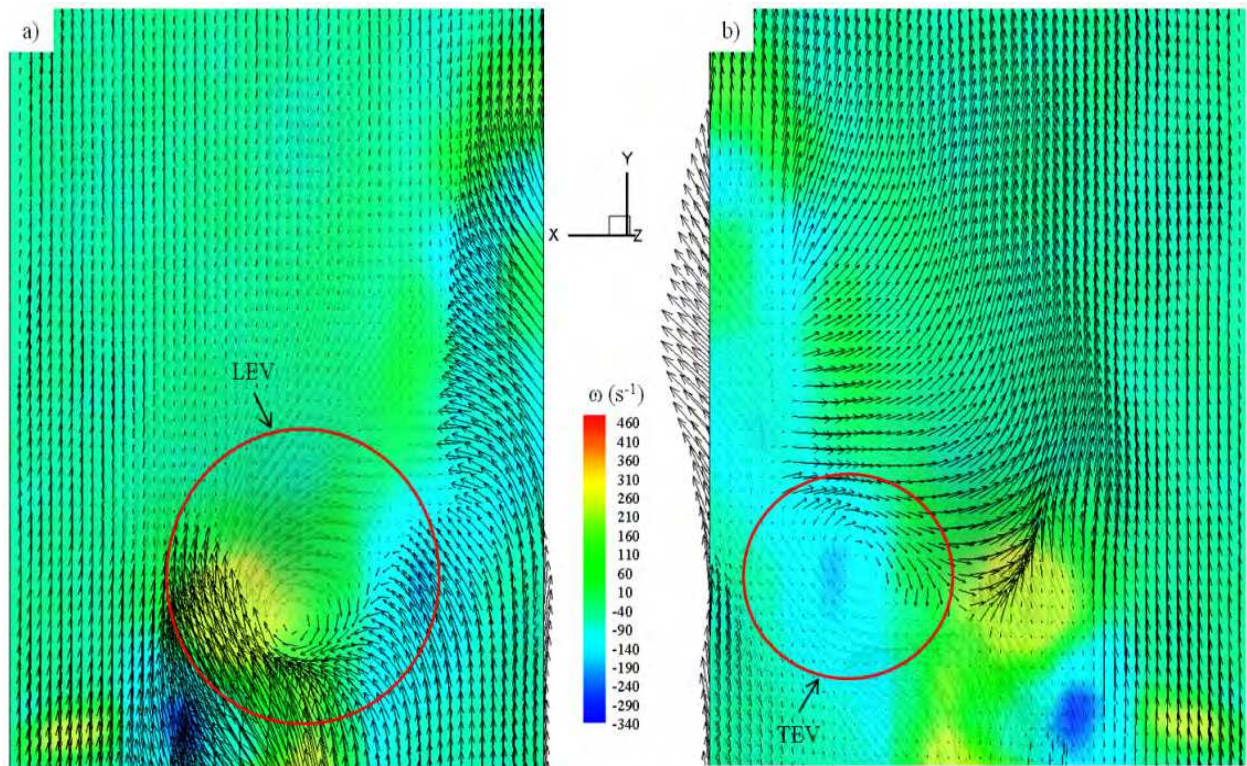


Fig. 11. Three dimensional instantaneous flow structure and vorticity contours displayed using Tecplot 360.

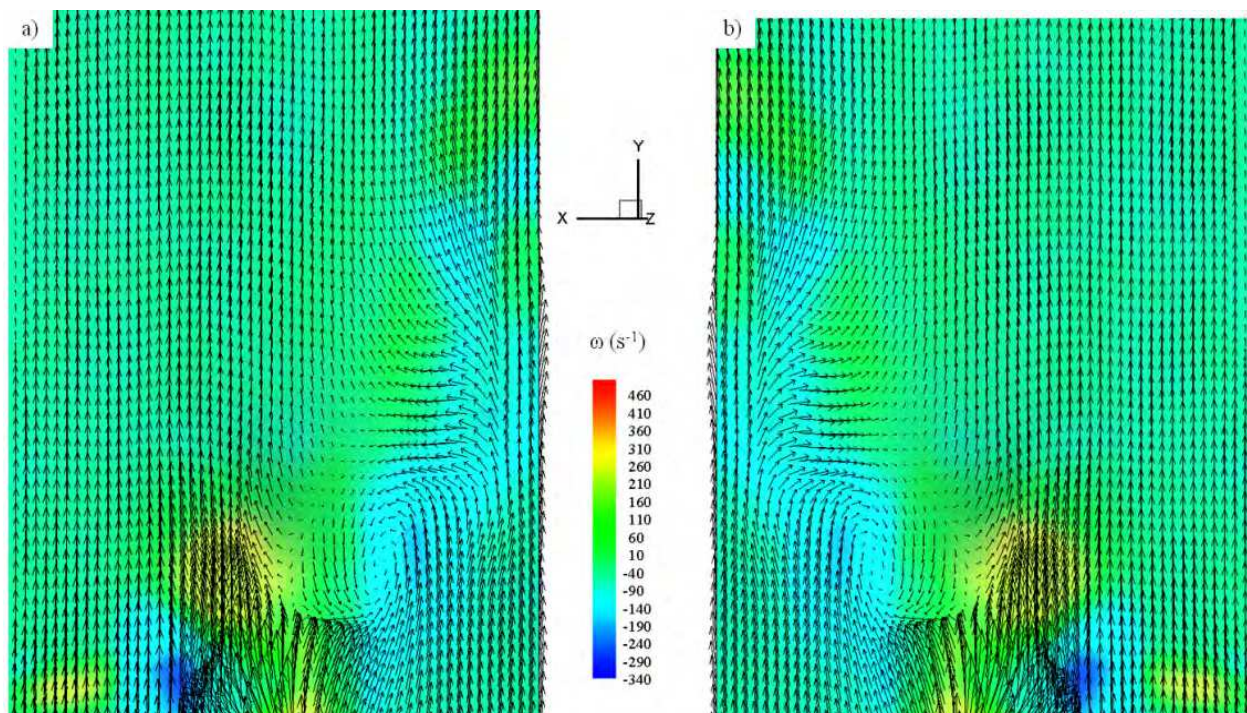


Fig. 12. Three dimensional instantaneous flow structure and vorticity contours projected onto a 2D plane and displayed using Tecplot 360.

## 5. Conclusion

Currently, the PIV technique is the standard method for measuring fluid flow velocity in a wide range of research and technology fields. Stereoscopic PIV is particularly well-suited for the study of biomedical flows (bifurcation flow phenomena in realistic lung models and heart valves), automotive industry (drag reduction, engine compartment flows and exhaust systems), aerospace industry (wind tunnel measurements for the study of wing design and trailing vortices), naval applications (propeller wake flow analysis), turbulent flow (jet mixing flows), combustion processes (fuel/air mixing, flame and fire research, jet propulsion, explosion research, exhaust control and swirl in combustion systems), oceanography (wave dynamics, sedimentation/particle transport, tidal modelling and river hydrology), design and optimization of electronic devices (thermal loading on electronic components), hydraulics and hydrodynamics (propulsion efficiency, pipe flows, channel flows and bubble dynamics), mixing processes, spray atomization, fluid structure interaction, vortex evolution and heat transfer studies. Nonetheless, one drawback of PIV is that it requires optical access for the light sheet as well as for the cameras, which may sometimes be difficult to ensure. In these cases, point based techniques such as pitot probes, Constant Temperature Anemometry (CTA), or numerical simulations are reliable tools for the measurement of flows. One major advantage is that 2D PIV systems can easily be expanded for 3D capabilities. Although commercial stereoscopic PIV systems equipped with a 3D traverse system are very expensive (at least US\$300K), their ease of use allows anyone to perform high quality measurements without the need of any formal training in fluid mechanics. The aim of the present chapter is to describe the experimental methodology to plan and design experiments, perform a successful stereoscopic calibration, quantify the accuracy of the latter, and process the acquired data. It is hoped that the established methodology will prove useful to those who intent to obtain high quality three-component velocity results.

## 6. References

- Adrian, R. J. (1991). "Particle-imaging techniques for experimental fluid mechanics." *Annual Review in Fluid Mechanics* 23: 261-304.
- Adrian, R. J. and C. S. Yao (1985). "Pulsed laser technique application to liquid and gaseous flows and the scattering power of seed materials." *Applied Optics* 24: 44-52.
- Arroyo, M. and C. Greated (1991). "Stereoscopic particle image velocimetry." *Measurement Science and Technology* 2: 1181-1186.
- Doorne, C. W. H. v. (2004). *Stereoscopic PIV on transition in pipe flow*. The Netherlands, Delft University of Technology. Ph.D. thesis.
- Ehrenfried, K. (2002). "Processing calibration grid images using the Hough transformation." *Measurement Science and Technology* 12: 975-983.
- Grant, I., Y. Zhao, et al. (1991). *Three component flow mapping: experiences in stereoscopic PIV and holographic velocimetry*. New York: ASME.
- Harrison, G. M., N. J. Lawson, et al. (2001). "The measurement of the flow around a sphere settling in a rectangular box using 3-dimensional particle image velocimetry." *Chemical Engineering Communications* 188: 143-178.

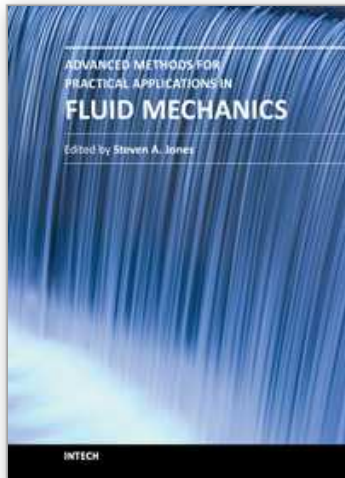
- Hinsch, K. D. (1993). "Three-dimensional particle image velocimetry." *Measurement Science and Technology* 6: 742-753.
- Hu, H. T. Saga, et al. (2001). "Dual-plane stereoscopic particle image velocimetry: system set-up and its application on a lobed jet mixing flow." *Experiments in Fluids* 31: 277-293.
- Jakobsen, M. L., T. P. Dewhurst, et al. (1997). "Particle image velocimetry for predictions of acceleration fields and force within fluid flows." *Measurement Science and Technology* 8: 1502-1516.
- Kähler, C. and J. Kompenhans (2000). "Fundamentals of multiple plane stereo particle image velocimetry." *Experiments in Fluids* 29: 70-77.
- Keane, R. D. and R. J. Adrian (1992). "Theory of cross correlation analysis of PIV images." *Journal of Applied Scientific Research* 49: 191-125.
- Klank, H., G. Goranovic, et al. (2001). "Micro PIV measurements in micro cell sorters and mixing structures with three-dimensional flow behaviour." *Proceedings of 4th International Symposium on Particle Velocimetry*. Göttingen, Institute of Aerodynamics and Flow Technology.
- Lawson, N. and J. Wu (1997). "Three-dimensional particle image velocimetry: error analysis of stereoscopic techniques." *Measurement Science and Technology* 8: 894-900.
- Lawson, N. J. and J. Wu (1997). "Three-dimensional particle image velocimetry: experimental error analysis of a digital angular stereoscopic system." *Measurement Science and Technology* 8: 1455-1464.
- Lawson, N. J. and J. Wu (1999). "Three-dimensional particle image velocimetry: a low-cost 35mm angular stereoscopic system for liquid flows." *Optics and Lasers in Engineering* 32: 1-19.
- Mao, Z. Q., N. A. Halliwell, et al. (1993). "Particle image velocimetry: high-speed transparency scanning and correlation-peak location in optical processing systems." *Applied Optics* 32(26): 5089-5091.
- Meinhart, C. D., S. T. Wereley, et al. (2000). "Volume illumination for two-dimensional particle image velocimetry." *Measurement Science and Technology* 11: 809-814.
- Melling, A. (1997). "Tracer particles and seeding for particle image velocimetry." *Measurement Science and Technology* 8: 1406-1416.
- Mullin, J. A. and W. J. A. Dahm (2005). "Dual-plane stereo particle image velocimetry (DSPIV) for measuring velocity gradient fields at intermediate and small scales of turbulent flows." *Experiments in Fluids* 38: 185-196.
- Mullin, J. A. and W. J. A. Dahm (2006). "Dual-plane stereo particle image velocimetry measurements of velocity gradient tensor fields in turbulent shear flow. I. Accuracy assessments." *Physics of Fluids* 18: 035101.
- Nishino, N., N. Kasagi, et al. (1989). "Three dimensional particle image velocimetry based on automated digital image processing." *Journal of Fluids Engineering* 111: 384-391.
- Perret, L., P. Braud, et al. (2006). "3-component acceleration field measurement by dual-time stereoscopic system." *Experiments in Fluids* 40: 813-824.

- Prasad, A. (2000). "Stereoscopic particle image velocimetry." *Experiments in Fluids* 29: 103-116.
- Prasad, A. K. and R. J. Adrian (1993). "Stereoscopic particle image velocimetry applied to liquid flows." *Experiments in Fluids* 15: 49-60.
- Prasad, A. K. and K. Jensen (1995). "Scheimpflug stereocamera for particle image velocimetry to liquid flows." *Applied Optics* 34: 7092-7099.
- Raffel, M., M. Gharib, et al. (1995). "Feasibility study of three-dimensional PIV by correlating images of particles within parallel light sheet planes." *Experiments in Fluids* 19(2): 69-77.
- Raffel, M., C. Willert, et al. (1998). *Particle Image Velocimetry A Practical Guide*. Berlin, Springer.
- Scheimpflug, T. (1904). Improved Method and Apparatus for the Systematic Alteration of Distortion of Plane Pictures and Images by Means of Lenses and Mirrors for Photography and for other purposes. B. P. N. 1196.
- Schröder, A. and J. Kompenhans (2004). "Investigation of a turbulent spot using multi-plane stereo particle image velocimetry." *Experiments in Fluids* 36: 82-90.
- Sinha, S. K. (1988). "Improving the accuracy and resolution of particle image or laser speckle velocimetry." *Experiments in Fluids* 6: 67-68.
- Soloff, S., R. J. Adrian, et al. (1997). "Distortion compensation for generalized stereoscopic particle image velocimetry." *Measurement Science and Technology* 8: 1441-1454.
- Tatum, J. A., M. V. Finniss, et al. (2005). "3-D particle image velocimetry of the flow field around a sphere sedimenting near a wall: Part 2. Effects of distance from the wall." *Journal of Non-Newtonian Fluid Mechanics* 127(2-3): 95-106.
- Tatum, J. A., M. V. Finniss, et al. (2007). "3D particle image velocimetry of the flow field around a sphere sedimenting near a wall: Part 1. Effects of Weissenberg number." *Journal of Non-Newtonian Fluid Mechanics* 141: 99-115.
- Westerweel, J. (1997). "Fundamentals of digital particle image velocimetry." *Measurement Science and Technology* 8: 1379-1392.
- Westerweel, J., D. Dabiri, et al. (1997). "The effect of a discrete window offset on the accuracy of cross-correlation analysis of digital PIV recordings." *Experiments in Fluids* 23: 20-28.
- Westerweel, J. and F. T. M. Nieuwstadt (1991). Performance tests on 3-dimensional velocity measurements with a two-camera digital particle-image velocimeter. ASME, New York, A. Dybbs and B. Ghorashi.
- Westerweel, J. and F. T. M. Nieuwstadt (1997). Performance tests on 3-dimensional velocity measurements with a two-camera digital particle-image velocimeter. Proceedings of the 4th International Conference in Laser Anemometry - Advances and Applications, Cleveland, OH.
- Wieneke, B. (2005). "Stereo-PIV using self-calibration on particle images." *Experiments in Fluids* 39: 267-280.
- Willert, C. (1997). "Stereoscopic particle image velocimetry for applications in wind tunnel flows." *Measurement Science and Technology* 8: 1465-1479.
- Willert, C. E. and M. Gharib (1991). "Digital particle image velocimetry." *Experiments in Fluids* 10: 181-193.

Zang, W. and A. K. Prasad (1997). "Performance evaluation of a Scheimpflug stereocamera for particle image velocimetry." *Applied Optics* 36(33): 8738-8744.

IntechOpen

IntechOpen



## **Advanced Methods for Practical Applications in Fluid Mechanics**

Edited by Prof. Steven Jones

ISBN 978-953-51-0241-0

Hard cover, 230 pages

**Publisher** InTech

**Published online** 14, March, 2012

**Published in print edition** March, 2012

Whereas the field of Fluid Mechanics can be described as complicated, mathematically challenging, and esoteric, it is also imminently practical. It is central to a wide variety of issues that are important not only technologically, but also sociologically. This book highlights a cross-section of methods in Fluid Mechanics, each of which illustrates novel ideas of the researchers and relates to one or more issues of high interest during the early 21st century. The challenges include multiphase flows, compressibility, nonlinear dynamics, flow instability, changing solid-fluid boundaries, and fluids with solid-like properties. The applications relate problems such as weather and climate prediction, air quality, fuel efficiency, wind or wave energy harvesting, landslides, erosion, noise abatement, and health care.

### **How to reference**

In order to correctly reference this scholarly work, feel free to copy and paste the following:

L. Martínez-Suástegui (2012). Overview on Stereoscopic Particle Image Velocimetry, *Advanced Methods for Practical Applications in Fluid Mechanics*, Prof. Steven Jones (Ed.), ISBN: 978-953-51-0241-0, InTech, Available from: <http://www.intechopen.com/books/advanced-methods-for-practical-applications-in-fluid-mechanics/overview-on-stereoscopic-particle-image-velocimetry>

**INTECH**  
open science | open minds

### **InTech Europe**

University Campus STeP Ri  
Slavka Krautzeka 83/A  
51000 Rijeka, Croatia  
Phone: +385 (51) 770 447  
Fax: +385 (51) 686 166  
[www.intechopen.com](http://www.intechopen.com)

### **InTech China**

Unit 405, Office Block, Hotel Equatorial Shanghai  
No.65, Yan An Road (West), Shanghai, 200040, China  
中国上海市延安西路65号上海国际贵都大饭店办公楼405单元  
Phone: +86-21-62489820  
Fax: +86-21-62489821

© 2012 The Author(s). Licensee IntechOpen. This is an open access article distributed under the terms of the [Creative Commons Attribution 3.0 License](#), which permits unrestricted use, distribution, and reproduction in any medium, provided the original work is properly cited.

IntechOpen

IntechOpen